Citation information: DOI 10.1109/TIE.2017.2733459, IEEE

Exponentially Stable Lyapunov Function Based Controller for Flyback CCM Converter

Seok-Min Wi, *Student Member, IEEE*, Jin S. Lee, *Member, IEEE*, and Minsung Kim, *Member, IEEE*

***Abstract*—In this paper, we propose a Lyapunov function based controller for the flyback converter operating in the continuous conduction mode (CCM). The controller consists of a duty-ratio feedforward control unit and a Lyapunov function based feedback control unit. The duty-ratio feedforward signal is used to reduce the burden from the Lyapunov feedback controller. The control system guarantees global exponential stability of the closed-loop system and hence offers fast transient response under large-signal perturbations. In constructing the controller, we use the average model of the flyback CCM converter taking the parasitic components into account. Numerical simulations confirmed its superior performance and experimental tests validated the proposed control approach.**

***Index Terms*—Lyapunov stability, nonlinear controller, nonlinear systems, dynamic response, parasitic components**

I. Introduction

THE dc/dc converters based on flyback topology have been widely used in the industrial areas such as electronic devices, telecommunication equipments, and automotive systems due to its design simplicity, cost effectiveness, and isolation characteristics [1–3]. The flyback dc/dc converter can be designed to operate either in the discontinuous conduction mode (DCM) or in the continuous conduction mode (CCM). The flyback converter operating in CCM is more efficient with lower current stress and easier to design a filter over those operating in DCM, and hence there have been considerable interests in using the flyback CCM converter for industrial applications [4–7]. However, it suffers from the nonminimum phase behavior because its transfer function from the control duty to the output voltage has the right-half-plane zero [8]. The output voltage control of the flyback CCM converter is a challenging issue.

With regard to control design of the flyback CCM converter, the linear control design techniques have been popular particularly when the converter operates around a fixed operating point. To design a linear controller systematically, we usually need a linearized model of the converter which cannot reflect the complete dynamic behavior of the flyback CCM converter. Due to this reason, it is usually difficult to stabilize the control system with the linear controller particularly under large perturbations from the operating point.

To overcome the problem, a number of researchers have proposed to use the nonlinear controllers to control the inherently nonlinear converter. It is developed directly from the nonlinear converter model and hence does not need any linearization process. A number of nonlinear control techniques such as backstepping control techniques, sliding mode control (SMC) techniques and model predictive control (MPC) techniques have been developed for the flyback CCM converter. The backstepping control is the stepwise control design technique based on the Lyapunov function and can regulate the output voltage of the converter by stabilizing the inductor current and guarantees closed-loop system stability [9]. But it is sensitive to parameter variations and suffers from slow transient response due to the inherent singularity problem. The SMC is a robust control technique that can cope with parameter variations, external disturbances, and unmodeled dynamics with fast transient performance. In its early stage, the hysteresis-modulation (HM)-based SMC has been widely used to regulate the output voltage of converters [10]. However, the HM-based SMC generates a bang-bang type control input, and so the controlled system generally suffers from chattering and significant switching-frequency variation when the input voltage and the output load are varied. These complicate the design of the input and output filters and deteriorate regulation properties of the converters. Thus, SMC that operates at constant switching frequency has been developed by employing pulse-width-modulation (PWM) instead of HM. An equivalent control is the low-frequency continuous switching action that will produce a trajectory that is of near equivalence to an ideal sliding mode trajectory [11]. This equivalent control can solve the drawbacks of the HM-based SMC such as the chattering and variable switching frequency problems. However, it would come with the steady-state error in the output voltage due to imperfect switching control action [12–14]. MPC offers a solution for trajectory optimization [15] but, because MPC calculates its control input from the dynamic model of the system, discrepancies between the actual system and the dynamic model such as uncertainties and external disturbances can deteriorate the performance of MPC. Moreover, due to large amount of computation in

Manuscript received January 8, 2017; revised April 1, 2017 and June 2, 2017; accepted July 10, 2017. This research was supported by the MSIP (Ministry of Science, ICT and Future Planning), Korea, under the "ICT Consilience Creative Program" (IITP-R0346-16-1007) supervised by the IITP (Institute for Information & communications Technology Promotion) and in part by the National Research Foundation of Korea (NRF) grant funded by MSIP (No. 2017R1C1B1003084).

S.-M. Wi is with Department of Electrical Engineering, Pohang University of Science and Technology (POSTECH), Pohang, 37673, Korea (e-mail: wsm7667@postech.ac.kr).

J. S. Lee, and M. Kim are with Department of Creative IT Engineering, Pohang University of Science and Technology (POSTECH), Pohang, 37673, Korea (e-mail: jsoo@postech.ac.kr; minsung.kim@postech.ac.kr).

Citation information: DOI 10.1109/TIE.2017.2733459, IEEE

the optimization process, MPC is not suitable for the high frequency switching converter.

The Lyapunov function based control strategy, which usually offers a solution that guarantees global asymptotic stability under large perturbations from the operating point. Motivated from the excellent properties of the Lyapunov function based control approach, this controller has been successfully implemented in the buck-boost converter [16], boost converter [17], single- and three-phase shunt active power filters [18, 19], single-phase grid-connected PV inverters [20], single-phase uninterruptible power system (UPS) inverters [21], single-phase grid-connected voltage source inverter (VSI) [22], and switched reluctance motor drive system [23]. In the Lyapunov function based control scheme, a control signal such that the total energy of the system is continuously dissipated has been designed. The state of the closed-loop system then converges to the equilibrium point.

In this paper, we propose a Lyapunov function based feedback controller to be used for the CCM flyback converter. The flyback CCM converter suffers from the nonminimum phase behavior due to the existence of right-half-plane zero in its transfer function. So, it shows poor transient response under the large signal perturbation. But, thanks to global exponential stable characteristic of Lyapunov function based controller, the transient response becomes significantly improved. To reduce the burden from the Lyapunov function based controller, we supplement it with the duty-ratio feedforward controller [24–26]. We take the parasitic components into account to develop the dynamic model of the flyback CCM converter, and use it to construct the proposed controller; it regulates the reference output voltage more accurately. We performed numerical simulations to demonstrate the superior performance and conducted experimental tests to validate the proposed control scheme.

This paper is organized as follows. We introduce the modeling of flyback converter with parasitic components in Section II. We present controller design and stability analysis in Section III. To validate the proposed controller, we show the simulation and experimental results in Section IV. Finally, we draw conclusions in Section V.

II. System Configuration

A. Modeling of the flyback CCM converter with parasitic components

Due to the difficulties and complexities of the modeling and controller design procedure, the parasitic components are usually ignored. The resultant ideal/lossless modeling significantly simplifies model development, and thereby contributes to understanding of the main features of the switching converter. However, the effects of parasitic components are important for improving the model accuracy and study of the dynamic performance. Use of a model that includes the parasitic components can improve steady-state performance as well as transient performance. Therefore, we take parasitic components into account to construct the dynamic model of the flyback CCM converter.

Fig. 1 describes the circuit diagram of the flyback converter with parasitic components. It consists of switch S_1,

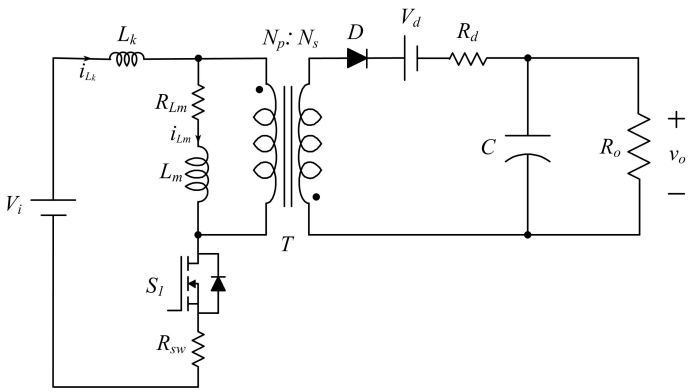

Fig. 1. Circuit diagram of the flyback CCM converter with parasitic components.

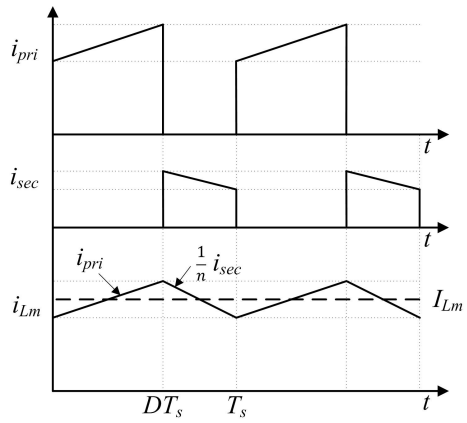

Fig. 2. Current waveforms of the flyback CCM converter.

transformer T with turns ratio $n = N_p/N_s$, magnetizing inductor L_m, diode D, and output capacitor C. The parasitic components are presented as leakage inductor L_k, the parasitic resistance of the switch R_{sw}, the direct current resistance of the magnetizing inductance R_{L_m}, the parasitic resistance of the diode R_d, and the voltage drop of the diode V_d; R_{sw} represents the resistance between the source and the drain of the switch during the switch on state [27, 28].

The flyback converter is operated as follows: when the switch is turned on, the magnetizing inductance of the transformer accumulates the electric energy from the input power source; when the switch is turned off, the stored energy then transfers to the secondary winding when the voltage direction is reversed; when the diode is turned on, the magnetizing energy transfers to the output capacitor and the load. Fig. 2 describes the waveforms of the primary current, secondary current, and magnetizing current. The magnetizing current increases when the switch is turned on. Otherwise, the magnetizing current decreases. Since the flyback converter is designed to operate in CCM, the magnetizing current never goes to zero during the switching period.

By applying Kirchhoff's voltage and current laws, the state-space equations corresponding to the switch turned-on or turned-off cases can be expressed in the following equations, respectively.

Citation information: DOI 10.1109/TIE.2017.2733459, IEEE

Switch turned-on:

$$(L_m + L_k)\frac{di_{Lm}}{dt} = -(R_{Lm} + R_{sw})i_{Lm} + V_i, \quad (1)$$

$$\frac{di_{Lk}}{dt} = \frac{di_{Lm}}{dt}, \quad (2)$$

$$C\frac{dv_o}{dt} = -\frac{1}{R_o}v_o, \quad (3)$$

Switch turned-off:

$$L_m\frac{di_{Lm}}{dt} = -(R_{Lm} + n^2R_d)i_{Lm} - nv_o - nV_d, \quad (4)$$

$$\frac{di_{Lk}}{dt} = 0, \quad (5)$$

$$C\frac{dv_o}{dt} = ni_{Lm} - \frac{1}{R_o}v_o, \quad (6)$$

where i_{Lm} is the current through the magnetizing inductor, i_{Lk} is the current through the leakage inductor, V_i is the input voltage, and v_o is the output voltage.

Combining (1) through (6) using the averaging technique, we obtained the average model that can be expressed as

$$\frac{d\bar{i}_{Lm}}{dt} = -\Big\{\frac{(R_{Lm} + R_{sw})u}{L_m + L_k} + \frac{1}{L_m}(n^2R_d + R_{Lm})(1-u)\Big\} \cdot \bar{i}_{Lm} - \frac{n(1-u)}{L_m}\bar{v}_o + \frac{V_iu}{L_m + L_k} - \frac{nV_d(1-u)}{L_m}, \quad (7)$$

$$\frac{d\bar{i}_{Lk}}{dt} = -\frac{(R_{Lm} + R_{sw})u}{L_m + L_k}\bar{i}_{Lk} + \frac{V_iu}{L_m + L_k}, \quad (8)$$

$$\frac{d\bar{v}_o}{dt} = \frac{n(1-u)}{C}\bar{i}_{Lm} - \frac{\bar{v}_o}{CR_o}, \quad (9)$$

where u is the control duty ($0 \le u \le 1$) and $\bar{i}_{Lm}$, $\bar{i}_{Lk}$ and $\bar{v}_o$ are average values of i_{Lm}, i_{Lk} and v_o during the switching period.

III. Controller Design and Stability Analysis

The control objective of the flyback CCM converter is to make the output voltage track the reference signal as closely as possible. Conventional proportional-integral (PI) control scheme is usually designed using the linearized model of the converter and has been widely used to stabilize the converter. But it shows poor transient response under large signal perturbations because the small signal model at each operating point is not accurate. To accomplish fast dynamic response and derive global exponential stability even under large signal perturbations, we propose to use a Lyapunov function based controller. To reduce the burden from the Lyapunov function based controller, we supplement it with the duty-ratio feedforward signal. In this section, we first develop the duty-ratio feedforward control part and use it to derive the error dynamics. The resulting error dynamic model is then used to develop the Lyapunov function based controller.

A. Duty-ratio feedforward controller

For subsequent development, we define the reference magnetizing inductor current as I_{Lm} and the reference output voltage as V_o and assume that the flyback CCM converter operates in the steady-state. Substituting I_{Lm} and V_o into $\bar{i}_{Lm}$ and $\bar{v}_o$, and setting $\frac{d\bar{i}_{Lm}}{dt} = 0$ and $\frac{d\bar{v}_o}{dt} = 0$ in the average model, we have

$$I_{Lm} = \frac{-\frac{n(1-u_{ff})V_o}{L_m} + \frac{V_iu_{ff}}{L_m+L_k} - \frac{nV_d(1-u_{ff})}{L_m}}{\frac{(R_{Lm}+R_{sw})u_{ff}}{L_m+L_k} + \frac{1}{L_m}(n^2R_d+R_{Lm})(1-u_{ff})}, \quad (10)$$

$$I_{Lk} = \frac{V_i}{R_{Lm} + R_{sw}}, \quad (11)$$

$$V_o = nR_o(1-u_{ff})I_{Lm}, \quad (12)$$

Multiplying both sides of (10) by $\frac{(R_{Lm}+R_{sw})u_{ff}}{L_m+L_k} + \frac{1}{L_m}\big(n^2R_d + R_{Lm}\big)(1-u_{ff})$ and rearranging (10), we have

$$\Big\{\frac{(R_{Lm} + R_{sw})u_{ff}}{L_m + L_k} + \frac{1}{L_m}\big(n^2R_d + R_{Lm}\big)(1-u_{ff})\Big\}I_{Lm} + \frac{n(1-u_{ff})}{L_m}V_o - \frac{V_iu_{ff}}{L_m + L_k} + \frac{nV_d(1-u_{ff})}{L_m} = 0. \quad (13)$$

Substituting (12) into (13), we then obtain

$$\Big\{\frac{(R_{Lm} + R_{sw})u_{ff}}{L_m + L_k} + \frac{1}{L_m}(n^2R_d + R_{Lm})(1-u_{ff})\Big\} \cdot \frac{V_o}{nR_o(1-u_{ff})} + \frac{n(1-u_{ff})}{L_m}V_o - \frac{V_iu_{ff}}{L_m + L_k} + \frac{nV_d(1-u_{ff})}{L_m} = 0. \quad (14)$$

which in turn can be arranged as

$$\begin{aligned}&\big\{-L_m(R_{Lm} + R_{sw})(1-u_{ff}) + L_m(R_{Lm} + R_{sw}) \\ &+ (L_m + L_k)(n^2R_d + R_{Lm})(1-u_{ff})\big\}\frac{V_o}{nR_o(1-u_{ff})} \\ &+ n(L_m + L_k)(1-u_{ff})V_o + L_mV_i(1-u_{ff}) - L_mV_i \\ &+ nV_d(L_m + L_k)(1-u_{ff}) = 0. \end{aligned} \quad (15)$$

Multiplying both sides of (15) by $nR_o(1-u_{ff})$ results in

$$\begin{aligned}&nR_o\big\{n(L_m + L_k)V_o + L_mV_i + n(L_m + L_k)V_d\big\}u_{ff}'^2 \\ &-\Big\{nR_oL_mV_i + L_m(R_{Lm} + R_{sw}) - (L_m + L_k) \\ &\cdot (n^2R_d + R_{Lm})V_o\Big\}u_{ff}' + L_m(R_{Lm} + R_{sw})V_o = 0 \end{aligned} \quad (16)$$

where $u_{ff}' = 1 - u_{ff}$. u_{ff}' can then be calculated from (16) as

$$u_{ff}' = \frac{G_1 \pm G_2}{G_3}, \quad (17)$$

where

$$G_1 = nR_oL_mV_i + L_m(R_{Lm} + R_{sw}) - (L_m + L_k)(n^2R_d + R_{Lm})V_o, \quad (18)$$

$$G_2 = \sqrt{\begin{aligned}&\big\{nR_oL_mV_i + L_m(R_{Lm} + R_{sw}) \\ &\quad - (L_m + L_k)(n^2R_d + R_{Lm})V_o\big\}^2 \\ &-4nR_oL_m(R_{Lm} + R_{sw})\big\{n(L_m + L_k) \\ &\quad \cdot V_o + L_mV_i + n(L_m + L_k)V_d\big\}V_o\end{aligned}}, \quad (19)$$

$$G_3 = 2nR_o\big\{n(L_m + L_k)V_o + L_mV_i + n(L_m + L_k)V_d\big\}. \quad (20)$$

Between the two values of u_{ff}', the one with the minus sign in the numerator makes the reference magnetizing current to

Citation information: DOI 10.1109/TIE.2017.2733459, IEEE

become too large. Thus, we use the following duty-ratio

$$u_{ff} = 1 - \frac{G_1 - G_2}{G_3}. \tag{21}$$

u_{ff} itself does not directly determine the output voltage of flyback CCM converter. It is used as a feedforward input so that the output voltage of the converter tracks the reference output voltage closely. In other words, the feedforward controller reduces the burden from the feedback controller, which therefore does not require a high gain in the feedback controller.

B. Lyapunov function based controller

To construct a Lyapunov function based controller, we first apply the duty-ratio feedforward signal u_{ff} to the converter and derive the error dynamics. We first define the magnetizing inductor current error as $e_i = \bar{i}_{Lm} - I_{Lm}$, the output capacitor error as $e_v = \bar{v}_o - V_o$, and the feedback control term as $u_{fb} = u - u_{ff}$. Substituting e_i, e_v, and u_{fb} into (7) and (9), we obtain

$$\begin{aligned}\dot{e}_i = &-\Big\{\frac{R_{Lm}+R_{sw}}{L_m+L_k}u_{ff} + \frac{1}{L_m}(n^2R_d + R_{Lm})(1-u_{ff})\Big\} \\ &\cdot e_i - \frac{n(1-u_{ff})}{L_m}e_v + \Big\{\Big(-\frac{R_{Lm}+R_{sw}}{L_m+L_k} + \frac{n^2R_d}{L_m} \\ &+ \frac{R_{Lm}}{L_m}\Big)e_i + \frac{n}{L_m}e_v + \Big(-\frac{R_{Lm}+R_{sw}}{L_m+L_k} + \frac{n^2R_d}{L_m} \\ &+ \frac{R_{Lm}}{L_m}\Big)I_{Lm} + \frac{n}{L_m}V_o + \frac{V_i}{L_m+L_k} + \frac{nV_d}{L_m}\Big\}u_{fb},\end{aligned} \tag{22}$$

$$\dot{e}_v = \frac{n(1-u_{ff})}{C}e_i - \frac{1}{CR_o}e_v - \Big\{\frac{n}{C}e_i + \frac{nI_{Lm}}{C}\Big\}u_{fb}, \tag{23}$$

The error dynamics (22) and (23) can be compactly described as

$$\dot{\mathbf{e}} = \mathbf{A}\mathbf{e} + (\mathbf{B}\mathbf{e} + \mathbf{b})u_{fb}, \tag{24}$$

where

$$\mathbf{e} = \begin{bmatrix} e_i \\ e_v \end{bmatrix}, \tag{25}$$

$$\mathbf{A} = \begin{bmatrix} -\frac{R_{Lm}+R_{sw}}{L_m+L_k}u_{ff} - \frac{(n^2R_d+R_{Lm})(1-u_{ff})}{L_m} & -\frac{n(1-u_{ff})}{L_m} \\ \frac{n(1-u_{ff})}{C} & -\frac{1}{CR_o} \end{bmatrix}, \tag{26}$$

$$\mathbf{B} = \begin{bmatrix} -\frac{R_{Lm}+R_{sw}}{L_m+L_k} + \frac{n^2R_d}{L_m} + \frac{R_{Lm}}{L_m} & \frac{n}{L_m} \\ -\frac{n}{C} & 0 \end{bmatrix}, \tag{27}$$

$$\mathbf{b} = \begin{bmatrix} \big(-\frac{R_{Lm}+R_{sw}}{L_m+L_k} + \frac{n^2R_d}{L_m} + \frac{R_{Lm}}{L_m}\big)I_{Lm} \\ +\frac{n}{L_m}V_o + \frac{1}{L_m+L_k}V_i + \frac{n}{L_m}V_d \\ -\frac{n}{C}I_{Lm} \end{bmatrix}. \tag{28}$$

According to the Lyapunov stability theorem [29], the closed-loop system becomes exponentially stable if the Lyapunov function $V(\mathbf{x})$ satisfies $c_1||\mathbf{x}||^a \le V(\mathbf{x}) \le c_2||\mathbf{x}||^a$ and $\dot{V}(\mathbf{x}) \le -c_3||\mathbf{x}||^a$ where $0 < c_1 < c_2$, $0 < c_3$ and a can be any positive constant.

If we choose the Lyapunov function candidate as the energy stored in the magnetizing inductor and output capacitor:

$$V(\mathbf{e}) = \frac{1}{2}L_m e_i^2 + \frac{1}{2}Ce_v^2 = \frac{1}{2}\mathbf{e}^T\mathbf{P}\mathbf{e}, \tag{29}$$

where $\mathbf{P} = diag\begin{bmatrix} L_m & C \end{bmatrix}$, then it holds that

$$\begin{aligned}\frac{1}{2}\min(L_m, C)||\mathbf{e}||_2^2 &= \frac{1}{2}\lambda_{\min}(\mathbf{P})||\mathbf{e}||_2^2 \le V(\mathbf{e}) \\ &\le \frac{1}{2}\lambda_{\max}(\mathbf{P})||\mathbf{e}||_2^2 = \frac{1}{2}\max(L_m, C)||\mathbf{e}||_2^2.\end{aligned} \tag{30}$$

Computing its derivative with respect to time, we obtain

$$\begin{aligned}\dot{V}(\mathbf{e}) &= \frac{1}{2}\dot{\mathbf{e}}^T\mathbf{P}\mathbf{e} + \frac{1}{2}\mathbf{e}^T\mathbf{P}\dot{\mathbf{e}} \\ &= \frac{1}{2}\{\mathbf{A}\mathbf{e} + (\mathbf{B}\mathbf{e}+\mathbf{b})u_{fb}\}^T \\ &\quad + \frac{1}{2}\mathbf{e}^T\mathbf{P}\{\mathbf{A}\mathbf{e} + (\mathbf{B}\mathbf{e}+\mathbf{b})u_{fb}\} \\ &= \frac{1}{2}\mathbf{e}^T(\mathbf{A}^T\mathbf{P} + \mathbf{P}\mathbf{A})\mathbf{e} + \frac{1}{2}u_{fb}\mathbf{e}^T(\mathbf{B}^T\mathbf{P} + \mathbf{P}\mathbf{B})\mathbf{e} \\ &\quad + u_{fb}\mathbf{b}^T\mathbf{P}\mathbf{e} \\ &= -\mathbf{e}^T\mathbf{Q}\mathbf{e} + u_{fb}\mathbf{e}^T\mathbf{K}\mathbf{e} + u_{fb}\mathbf{b}^T\mathbf{P}\mathbf{e},\end{aligned} \tag{31}$$

where

$$\begin{aligned}\mathbf{Q} &= -\frac{1}{2}(\mathbf{A}^T\mathbf{P} + \mathbf{P}\mathbf{A}) \\ &= \begin{bmatrix} \frac{L_m(R_{Lm}+R_{sw})}{L_m+L_k}u_{ff} \\ \quad + (n^2R_d + R_{Lm})(1-u_{ff}) & 0 \\ 0 & \frac{1}{R_o} \end{bmatrix} > 0,\end{aligned} \tag{32}$$

$$\begin{aligned}\mathbf{K} &= \frac{1}{2}(\mathbf{B}^T\mathbf{P} + \mathbf{P}\mathbf{B}) \\ &= \begin{bmatrix} -\frac{L_m(R_{Lm}+R_{sw})}{L_m+L_k} \\ \quad + \big(n^2R_d + R_{Lm}\big) & 0 \\ 0 & 0 \end{bmatrix}.\end{aligned} \tag{33}$$

When we choose a Lyapunov function based feedback controller as

$$u_{fb} = -\alpha(\mathbf{e}^T\mathbf{K}\mathbf{e} + \mathbf{b}^T\mathbf{P}\mathbf{e}), \tag{34}$$

where $\alpha > 0$, the time derivative of the Lyapunov function becomes

$$\begin{aligned}\dot{V}(\mathbf{e}) &= -\mathbf{e}^T\mathbf{Q}\mathbf{e} - \alpha(\mathbf{e}^T\mathbf{K}\mathbf{e} + \mathbf{b}^T\mathbf{P}\mathbf{e})^2 \\ &\le -\mathbf{e}^T\mathbf{Q}\mathbf{e} \\ &\le -\lambda_{\min}(\mathbf{Q})||\mathbf{e}||_2^2 \\ &= -\min\left(\begin{matrix}\frac{L_m(R_{Lm}+R_{sw})}{L_m+L_k}u_{ff} \\ \quad + (n^2R_d + R_{Lm})(1-u_{ff})\end{matrix}, \quad \frac{1}{R_o}\right)||\mathbf{e}||_2^2 \\ &< 0.\end{aligned} \tag{35}$$

From (30) and (35), we can conclude from the Lyapunov stability theorem that $e_i \to 0$ and $e_v \to 0$ exponentially fast as $t \to \infty$. In fact, combining (30) and (35), we obtain

$$\dot{V}(\mathbf{e}) \le -\frac{2\lambda_{\min}(\mathbf{Q})}{\lambda_{\max}(\mathbf{P})}V(\mathbf{e}), \tag{36}$$

Citation information: DOI 10.1109/TIE.2017.2733459, IEEE

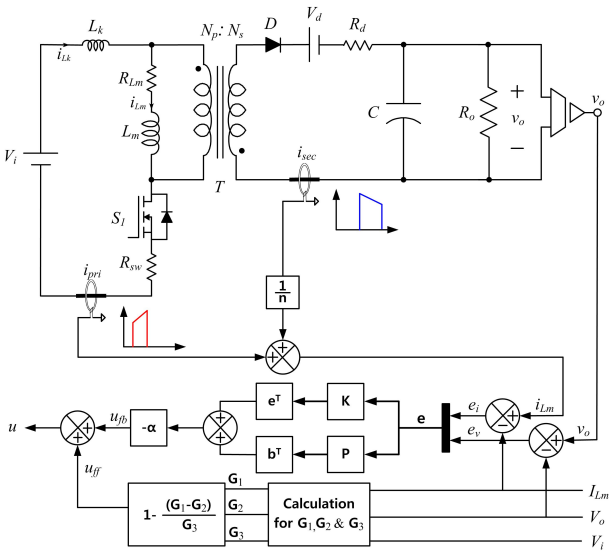

Fig. 3. Proposed control system of the flyback CCM converter.

and solving (36) gives

$$V(\mathbf{e}(t)) \le V(\mathbf{e}(t_0)) \exp\left\{ -\frac{2\lambda_{\min}(\mathbf{Q})}{\lambda_{\max}(\mathbf{P})}(t-t_0)\right\}, \quad (37)$$

for all $t \ge t_0$. Then the error trajectory is bounded as

$$\begin{aligned} ||\mathbf{e}||_2 &\le \left\{ \frac{2V(\mathbf{e}(t))}{\lambda_{\min}(\mathbf{P})} \right\}^{1/2} \\ &\le \left[\frac{2V(\mathbf{e}(t_0)) \exp\left\{ -\frac{2\lambda_{\min}(\mathbf{Q})}{\lambda_{\max}(\mathbf{P})}(t-t_0)\right\}}{\lambda_{\min}(\mathbf{P})} \right]^{1/2} \\ &\le \left[\frac{\lambda_{\max}(\mathbf{P})||\mathbf{e}(t_0)||_2^2 \exp\left\{ -\frac{2\lambda_{\min}(\mathbf{Q})}{\lambda_{\max}(\mathbf{P})}(t-t_0)\right\}}{\lambda_{\min}(\mathbf{P})} \right]^{1/2} \\ &= \left\{ \frac{\lambda_{\max}(\mathbf{P})}{\lambda_{\min}(\mathbf{P})} \right\}^{1/2} ||\mathbf{e}(t_0)||_2 \exp\left\{ -\frac{\lambda_{\min}(\mathbf{Q})}{\lambda_{\max}(\mathbf{P})}(t-t_0)\right\}. \end{aligned} \quad (38)$$

Consequently, the error trajectories converge to zero exponentially fast with the rate of $-\frac{\lambda_{\min}(\mathbf{Q})}{\lambda_{\max}(\mathbf{P})}$.

The complete control input is then determined from (21) and (34) as

$$\begin{aligned} u &= u_{ff} + u_{fb} \\ &= 1 - \frac{G_1 - G_2}{G_3} - \alpha(\mathbf{e}^T\mathbf{K}\mathbf{e} + \mathbf{b}^T\mathbf{P}\mathbf{e}). \end{aligned} \quad (39)$$

The proposed control scheme (Fig. 3) consists of two components: the duty-ratio feedforward control term that helps the output voltage to track the reference voltage, and the Lyapunov function based feedback control term that drives the closed-loop system to become exponentially stable.

In order to design the proposed controller, we need to measure the current through the magnetizing inductor. The magnetizing inductor current is not usually measurable directly. But, as shown in Fig. 2, i_{Lm} can be expressed as the sum of i_{pri} and i_{sec}/n, and we can then determine i_{Lm} by

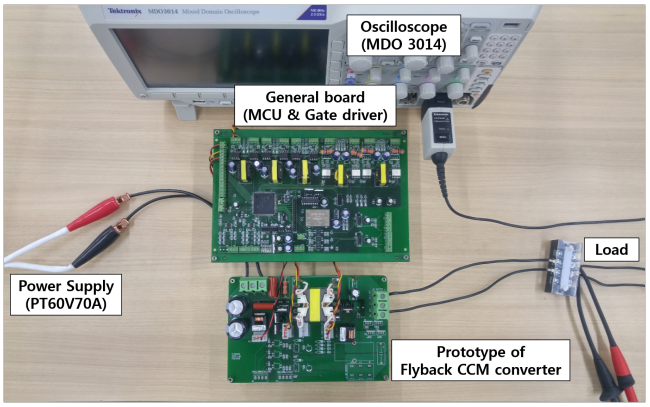

Fig. 4. Experimental setup of the flyback CCM converter.

TABLE I
PARAMETERS AND COMPONENTS OF THE FLYBACK CCM CONVERTER

Parameters	Symbols	Value
Transformer turns ratio	N_p:N_s	15:15
Magnetizing inductance	L_m	150 uH
Leakage inductance	L_k	1.3 uH
Output capacitance	C	300 uF
Switching frequency	f_s	50 kHz
Magnetizing resistance	R_{Lm}	0.05 Ω
Switch resistance	R_{sw}	0.02 Ω
Diode resistance	R_d	0.1 Ω
Diode voltage drop	V_d	1.6 V
Components	**Symbols**	**Part number**
MOSFET	S_1	IPP200N25N3G
Transformer core	T	PQ3535
Diode	D	C2D05120A

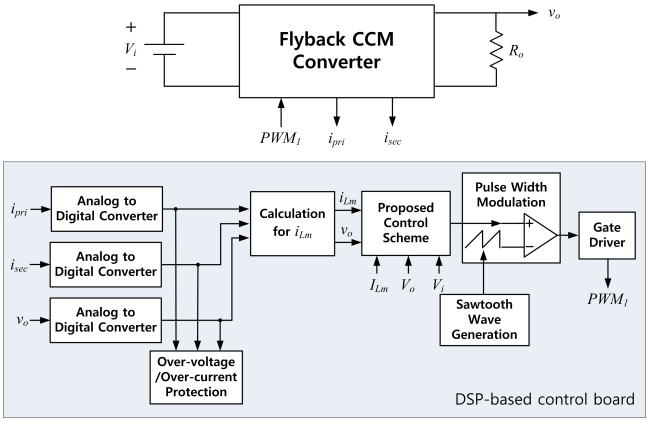

Fig. 5. Configuration of the proposed control system.

measuring i_{pri} and i_{sec}. Another approach is to adopt the state observer that can estimate the magnetizing current thereby removing the need to use the two current sensors. In this paper, we focus on demonstrating the feasibility of the proposed control scheme and simply assume that we use two current sensors instead of developing a state observer technique.

IV. Simulation and Experimental Results

In order to examine the transient response of the closed-loop system under variations of the reference output voltage,

 Citation information: DOI 10.1109/TIE.2017.2733459, IEEE

input voltage, and output load, we first conducted simulation tests using the computer simulation software PowerSim V9.0 (PSIM). Next, we carried out experimental tests using the prototype of the flyback CCM converter controlled by TMS320F28377D digital signal processor (Fig. 4). The major parameters of the flyback CCM converter are listed in Table I and the total system configuration is shown in Fig. 5.

To verify the performance of the proposed controller, we have compared the proposed controller with the voltage-mode controller, the current-mode controller, and the sliding mode controller. Type-II control scheme is adopted to construct the voltage mode controller for the flyback CCM converter.

$$G_{vc}(s) = \frac{k_{vc}}{s} \cdot \frac{s + w_{vc.z}}{s + w_{vc.p}}, \tag{40}$$

where k_{vc} is the integral gain of the voltage-mode controller, $w_{vc.z}$ is the zero of the voltage-mode controller, and $w_{vc.z}$ is the pole of the voltage-mode controller. Parameters of the voltage-mode controller were first set to satisfy the design criterion: the phase margin 55.9° and the closed-loop bandwidth 3.76 kHz; k_{vc}, $w_{vc.z}$, and $w_{vc.p}$ were set to 0.002, 3.5 and 300. We tested the control performance of the voltage-mode controller by changing the parameters around the preset value. Since we conducted the parameter optimization process, we obtained considerably improved result when k_{vc}, $w_{vc.z}$ and $w_{vc.p}$ were set to 0.004, 4.5 and 180 in the simulation test. As we selected the control parameters in experiment, a similar tendency was observed in the control performance of simulation and experiment. We obtained the experimental result when k_{vc}, $w_{vc.z}$ and $w_{vc.p}$ were set to 0.001, 7.1, and 210.

The current-mode controller consists of the inner-loop current controller and the outer-loop voltage controller. The controller structure in the outer voltage loop is the same as that in voltage-mode controller.

$$G_{cc}(s) = \frac{k_{cc}}{s} \cdot \frac{s + w_{cc.z}}{s + w_{cc.p}}, \tag{41}$$

where k_{cc} is the integral gain of the current-mode controller, $w_{cc.z}$ is the zero of the current-mode controller, and $w_{cc.z}$ is the pole of the current-mode controller. Parameters of the current-mode controller were first set to satisfy the design criterion: the phase margin 77.4° and the closed-loop bandwidth 3.9 kHz; k_{cc}, $w_{cc.z}$, and $w_{cc.p}$ were set to 0.1, 2.5 and 150. Using the same manner as in voltage-mode controller, we finally obtained k_{cc}, $w_{cc.z}$ and $w_{cc.p}$ as 0.3, 2.3 and 140 in the simulation and 0.6, 5.0 and 170 in experiment. These algorithms are built on TMS320F28377D microcontroller, which offers advantages of lower sensitivity to parameter variation, programmability and possibilities to improve performance using more advanced control schemes [30].

PWM based sliding mode controller is adopted to construct the sliding mode controller as in [33]. The sliding surface has been selected as

$$S = \lambda_1 e_i + \lambda_2 e_v + \lambda_3 \int e_i dt + \lambda_4 \int e_v dt, \tag{42}$$

where e_i and e_v are current and voltage errors, and λ_1, λ_2, λ_3 and λ_4 are positive constants.

Since the system has been linearized around the equilibrium point, root-locus technique is first used to analyze the effect of the parameters [31–33]. For parameter λ_1 and λ_2, the eigenvalues go close to real axis but do not go to the right-half plane as λ_1 and λ_2 increase respectively. For parameter λ_3, the eigenvalues go to minus infinity as λ_3 increases. For parameter λ_4, the eigenvalues lie in the open left-half complex plane with complex roots as λ_4 increases. Thus, with any positive parameter values, all of the eigenvalues lie in the open left-half complex plane and the linearized system is stable. Next, the parameters of the sliding mode controller were first determined to satisfy the design criterion: the phase margin 93.9° and the bandwidth 8.38 kHz; λ_1, λ_2, λ_3 and λ_4 were set to 0.001, 0.025, 3.2 and 6.8 respectively. Then, we tested the control performance of the sliding mode controller by changing the parameters around the preset value. Since we conducted the parameter optimization process, we obtained λ_1, λ_2, λ_3 and λ_4 as 0.005, 0.039, 2.0 and 6.5 in the simulation and 0.017, 0.04, 4.5 and 7.0 in the experiment.

For the proposed controller, we tested the performance of the controller by increasing the value of α. Since we did the parameter tuning process of proposed controller, we obtained the controller gain $\alpha = 0.004$ in the simulation and $\alpha = 0.002$ in the experiment.

A. Simulation Results

Simulation tests were performed to examine the transient response of the closed-loop system under variations of the reference output voltage, input voltage, and output load. The reference output voltage changed from 21 V to 15 V under the input voltage V_i = 12 V and the resistive load R_o = 20 Ω. The reference output voltage V_o was set to 21 V during the first 0.1 s, to 15 V during the next 0.1 s, and to 21 V during the rest 0.1 s. The input voltage changed from 10 V to 15 V under the reference output voltage V_o = 18 V and the resistive load R_o = 20 Ω. The input voltage V_i was set to 10 V during the first 0.1 s, to 15 V during the next 0.1 s, and to 10 V during the rest 0.1 s. The output load changed from 10 Ω to 20 Ω under the reference output voltage V_o = 18 V and the input voltage V_i = 12 V. The output load R_o was set to 20 Ω during the first 0.1 s, to 10 Ω during the next 0.1 s, to 20 Ω during the rest 0.1 s.

Fig. 6 shows the waveforms of the actual and reference output voltages under reference output voltage variations. As shown in Fig. 6(a), the actual output voltage tracks the reference output voltage rather slowly when the voltage-mode controller is used. Fig. 6(b) shows the waveforms of the actual and reference output voltages when the current-mode controller is used. Comparing the waveforms of Fig. 6(b) with those of Fig. 6(a), we see that the actual output voltage tracks the reference output voltage faster but its settling time is still too long. Fig. 6(c) shows the waveforms of the actual and reference output voltages when the sliding mode controller is used. The actual output voltage shows large overshoot and some oscillation before settling down to the reference output

Citation information: DOI 10.1109/TIE.2017.2733459, IEEE

voltage but its settling time is faster than that of Fig. 6(a) and Fig. 6(b). Fig. 6(d) shows the waveforms of the actual and reference output voltages when the proposed controller is applied. The output voltage indeed tracks the reference output voltage with significantly reduced overshoot and settling time. Fig. 7 shows the waveforms of the actual and reference output voltages under input voltage variations. A similar tendency is observed in the output voltage under input voltage variations. Fig. 8 shows the waveforms of the the actual and reference output voltages under output load variations. Here, the voltage-mode controller works better than the current-mode controller. It is due to the fact that the output impedance of the closed-loop system under voltage-mode control is smaller than that under current-mode control. When the sliding mode controller is used, the output voltage shows less peak behavior (Fig. 8(c)). When the proposed controller is used, the output voltage keeps its value well even under load variations (Fig. 8(d)).

To demonstrate the performance quality of the proposed controller, we examined the rise time and settling time of the transient responses under reference output voltage variations, the percentage of overshoot and settling time under input voltage variations, and the percentage of overshoot and settling time under output load variations (Tables II,III, and IV). The proposed controller exhibits the fastest and most stable step response among different types of controllers.

TABLE II
RISE TIME AND SETTLING TIME OF SIMULATION UNDER REFERENCE OUTPUT VOLTAGE VARIATION FOR EACH CONTROLLER

Controller	Rise time	Settling time
Voltage-mode controller	9.7 ms	12.9 ms
Current-mode controller	6.2 ms	9.0 ms
Sliding mode controller	1.2 ms	3.1 ms
Proposed controller	0.8 ms	2.0 ms

TABLE III
PERCENTAGE OF OVERSHOOT (PO) AND SETTLING TIME OF SIMULATION UNDER INPUT VOLTAGE VARIATION FOR EACH CONTROLLER

Controller	PO	Settling time
Voltage-mode controller	30.8 %	10.2 ms
Current-mode controller	18.7 %	8.8 ms
Sliding mode controller	9.8 %	3.2 ms
Proposed controller	6.4 %	1.6 ms

TABLE IV
PERCENTAGE OF OVERSHOOT (PO) AND SETTLING TIME OF SIMULATION UNDER OUTPUT LOAD VARIATION FOR EACH CONTROLLER

Controller	PO	Settling time
Voltage-mode controller	18.8 %	5.2 ms
Current-mode controller	20.9 %	7.9 ms
Sliding mode controller	10.6 %	2.0 ms
Proposed controller	5.4 %	0.7 ms

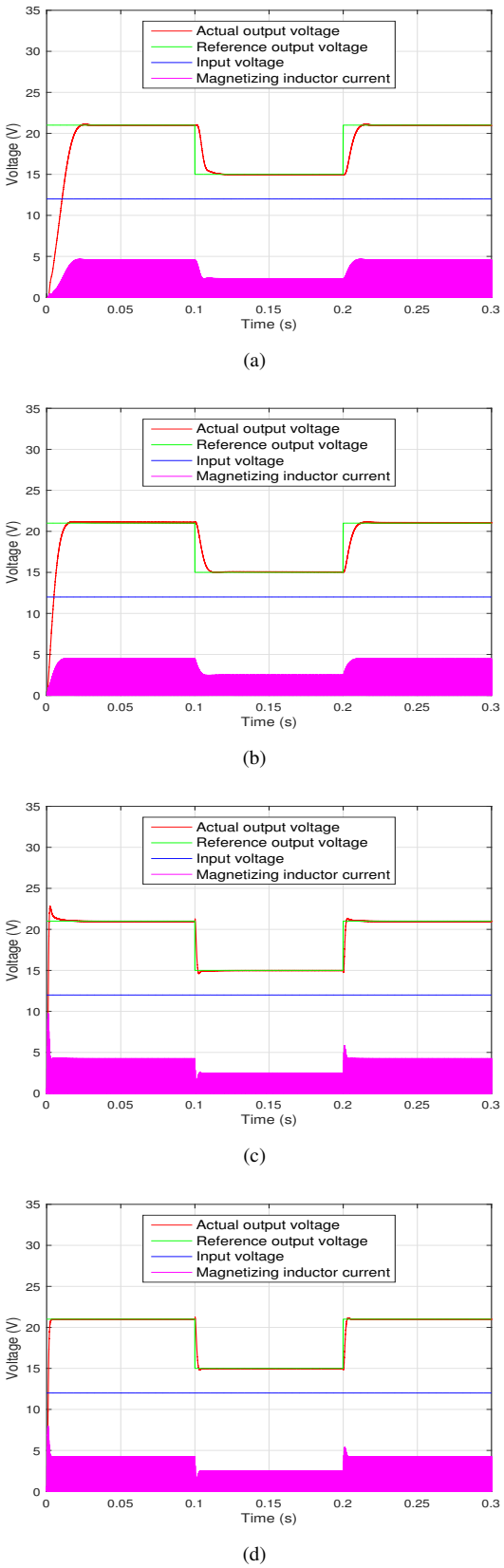

Fig. 6. Simulation waveforms of the flyback CCM converter under reference output voltage variations. (a) when the voltage-mode controller is used. (b) when the current-mode controller is used. (c) when the sliding mode controller is used. (d) when the proposed controller is used.

B. Experimental Results

The experiment was also performed to test the transient response of the closed-loop system under variations of the

Citation information: DOI 10.1109/TIE.2017.2733459, IEEE

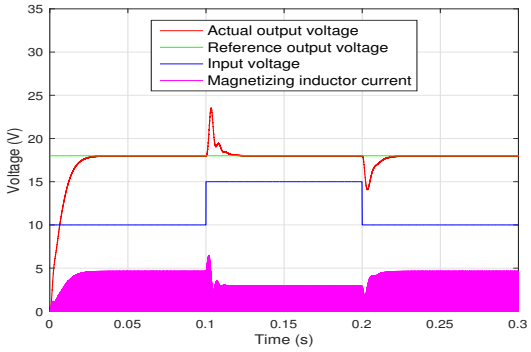

(a)

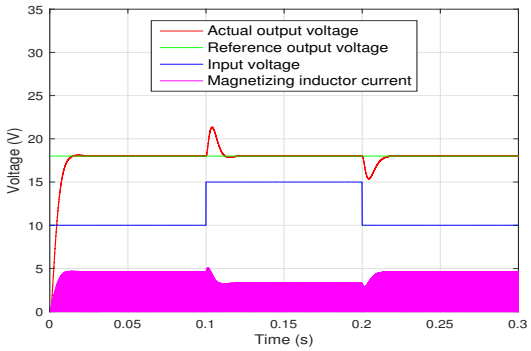

(b)

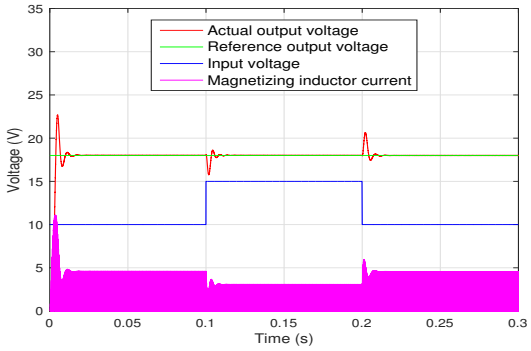

(c)

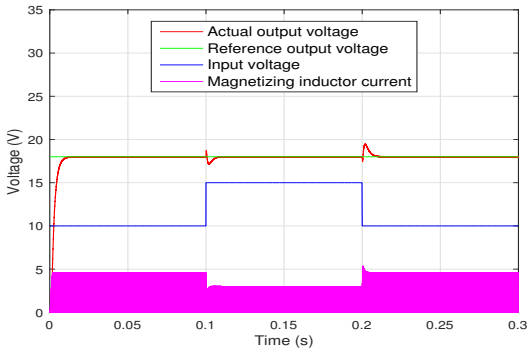

(d)

Fig. 7. Simulation waveforms of the flyback CCM converter under input voltage variations. (a) when the voltage-mode controller is used. (b) when the current-mode controller is used. (c) when the sliding mode controller is used. (d) when the proposed controller is used.

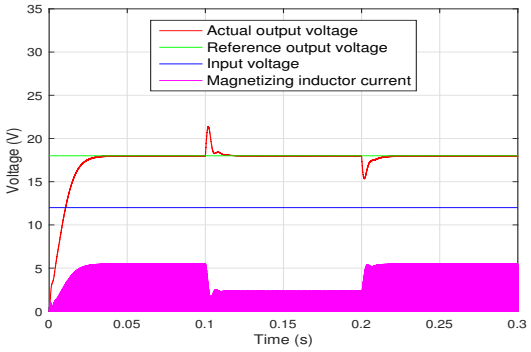

(a)

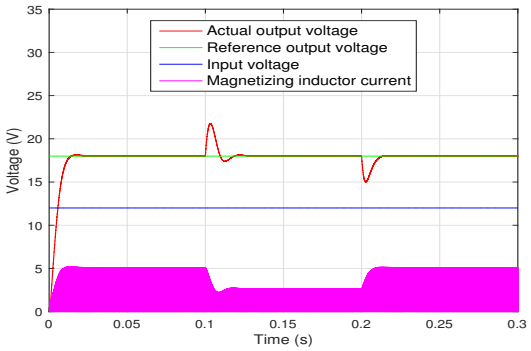

(b)

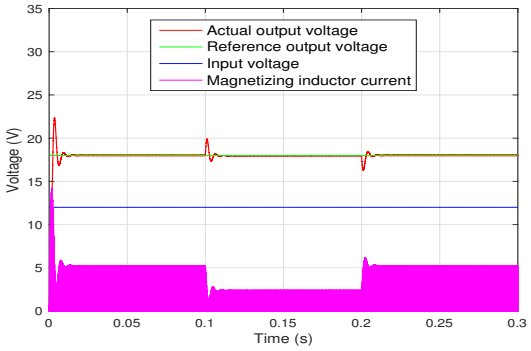

(c)

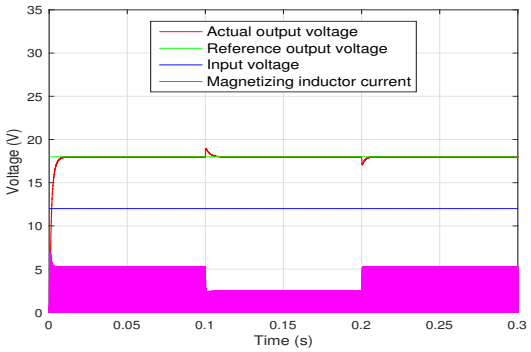

(d)

Fig. 8. Simulation waveforms of the flyback CCM converter under output load variations. (a) when the voltage-mode controller is used. (b) when the current-mode controller is used. (c) when the sliding mode controller is used. (d) when the proposed controller is used.

Citation information: DOI 10.1109/TIE.2017.2733459, IEEE

reference output voltage, input voltage, and output load. The reference output voltage is 2.5-Hz square-wave voltage that jumps between 21 V to 15 V. The input voltage is 2.5-Hz square-wave voltage that jumps between 10 V to 15 V. The output load is 2.5-Hz square-wave that jumps between 10 Ω to 20 Ω.

Fig. 9 shows the waveforms of the input/output voltages and inductor current under reference output voltage variations. As shown in Fig. 9(a), the output voltage tracks the reference output voltage rather slowly when the voltage-mode controller is used. Fig. 9(b) shows the waveforms of the input/output voltages and inductor current when the current-mode controller is used. Comparing the waveforms of Fig. 9(b) with those of Fig. 9(a), we see that the output voltage tracks the reference output voltage faster but its settling time is still too long. Even though we increase the controller gain to improve the transient performance, we cannot noticeably improve the transient response. Fig. 9(c) shows the waveforms of the input/output voltages and inductor current when the sliding mode controller is used. The output voltage tracks the reference output voltage with an acceptably short settling time. Fig. 9(d) shows the waveforms of the input/output voltages and inductor current when the proposed controller is applied. Thanks to the global exponential stability property of the proposed controller, the output voltage is able to track the reference output voltage well even during the transient period. Fig. 10 and Fig. 11 show the waveforms of the input/output voltages and inductor current under input voltage variations and output load variations. In agreement with simulation results, a similar tendency is observed in the waveforms. Fig. 12 shows the waveforms of the input/output voltages during the converter startup. During the startup transient, the proposed controller quickly tracks the reference output voltage without overshoot.

We alse examined the rise time and settling time of the transient responses under reference output voltage variations, the percentage of overshoot and settling time under input voltage variations, and the percentage of overshoot and settling time under output load variations (Tables V,VI, and VII). The proposed controller also shows the fastest and most stable step response among different types of controllers.

TABLE V
RISE TIME AND SETTLING TIME OF EXPERIMENT UNDER REFERENCE OUTPUT VOLTAGE VARIATION FOR EACH CONTROLLER

Controller	Rise time	Settling time
Voltage-mode controller	10.7 ms	13.7 ms
Current-mode controller	7.4 ms	10.2 ms
Sliding mode controller	0.9 ms	1.7 ms
Proposed controller	0.8 ms	1.2 ms

V. CONCLUSION

In this paper, we proposed a Lyapunov function based controller for the CCM flyback converter with design simplicity, cost effectiveness and isolation characteristics in mind. The Lyapunov function based controller guarantees global exponential stability of the closed-loop system and it provides fast transient response under the large-signal perturbations.

TABLE VI
PERCENTAGE OF OVERSHOOT (PO) AND SETTLING TIME OF EXPERIMENT UNDER INPUT VOLTAGE VARIATION FOR EACH CONTROLLER

Controller	PO	Settling time
Voltage-mode controller	37.3 %	19.1 ms
Current-mode controller	26.7 %	13.4 ms
Sliding mode controller	12.2 %	7.6 ms
Proposed controller	9.1 %	3.5 ms

TABLE VII
PERCENTAGE OF OVERSHOOT (PO) AND SETTLING TIME OF EXPERIMENT UNDER OUTPUT LOAD VARIATION FOR EACH CONTROLLER

Controller	PO	Settling time
Voltage-mode controller	11.3 %	11.5 ms
Current-mode controller	12.7 %	13.6 ms
Sliding mode controller	7.3 %	4.3 ms
Proposed controller	5.2 %	1.1 ms

To reduce the burden from the Lyapunov function based controller, we supplement it with the duty-ratio in the feed-forward loop. To achieve accurate control, we derive the average model of the flyback CCM converter taking the parasitic components into account and use the derived model to develop the controller; it regulates the reference output voltage more accurately. Numerical simulations confirmed its superior performance and experimental tests validated the proposed control approach.

REFERENCES

[1] W. -S. Liu, J. -F. Chen, T. -J. Liang, R. -L. Lin, and C. -H. Liu, "Analysis, design, and control of bidirectional cascoded configuration of a fuel cell hybrid power system," *IEEE Trans. Power Electron.*, vol. 25, no. 6, pp. 1565-1575, Jun. 2010.

[2] A. M. Imtiaz and F. H. Khan, "Time shared flyback converter based regenerative cell balancing technique for series connected Li-ion battery strings," *IEEE Trans. Power Electron.*, vol. 28, no. 12, pp. 5960-5975, Dec. 2013.

[3] D. G. Lamar, M. Arias, A. Rodriguez, A. Fernandez, M. M. Hernando, and J. Sebastian, "Design-oriented analysis and performance evaluation of a low-cost high-brightness LED driver based on flyback power factor corrector," *IEEE Trans. Ind. Electron.*, vol. 60, no. 7, pp. 2614-2626, Jul. 2013.

[4] N. P. Papanikolaou and E. C. Tatakis, "Active voltage clamp in flyback converters operating in CCM mode under wide load variation," *IEEE Trans. Ind. Electron.*, vol. 51, no. 3, pp. 632-640, Jun. 2004.

[5] D. M. Bellur, N. Kondrath, and M. K. Kazimierczuk, "Transformer winding loss caused by skin and proximity effects including harmonics in pulse-width modulated DC-DC flyback converters for the continuous conduction mode," *IET Power Electron.*, vol. 4, no. 4, pp. 363-373, Apr. 2011.

[6] J. Park, Y. -S. Roh, Y. -J. Moon, and C. Yoo, "A CCM/DCM dual-mode synchronous rectification controller for a high-efficiency flyback converter," *IEEE Trans. Power Electron.*, vol. 29, no. 2, pp. 768-774, Feb. 2014.

[7] K. Soltanzadeh, H. Khalilian, and M. Dehghani, "Analysis, design, and implementation of a zero voltage switching two-switch CCM flyback converter," *IET Circuits, Devices & Syst.*, vol. 10, no. 1, pp. 20-28, Jan. 2016.

[8] M. -C. Lee, J. -B. Lio, D. Y. Chen, Y. -T. Chen, and Y. -P. Wu, "Small-signal modeling of multiple-output flyback converters in continuous conduction mode with weighted feedback,"

Citation information: DOI 10.1109/TIE.2017.2733459, IEEE

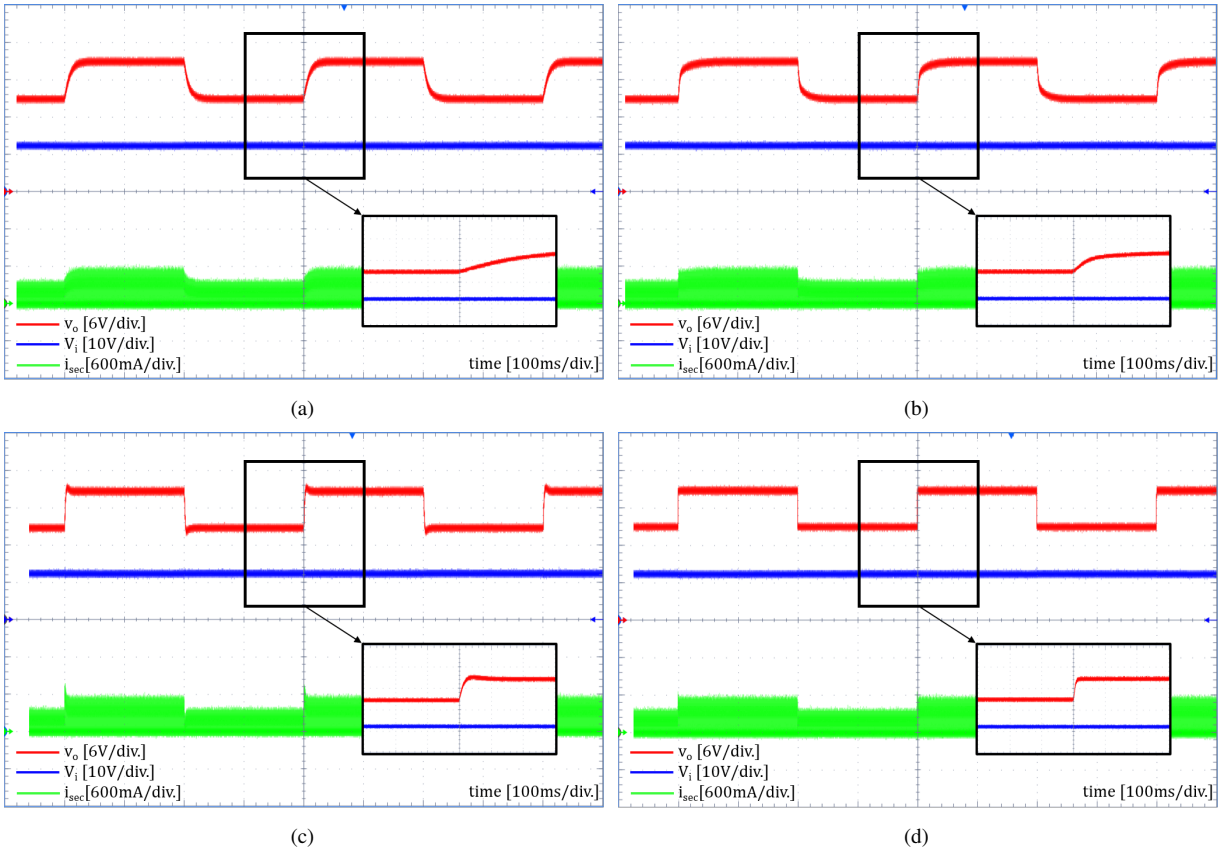

Fig. 9. Experimental waveforms of the flyback CCM converter under reference output voltage variations. (a) when the voltage-mode controller is used. (b) when the current-mode controller is used. (c) when the sliding mode controller is used. (d) when the proposed controller is used.

IEEE Trans. Ind. Electron., vol. 45, no. 2, pp. 236-248, Apr. 1998.

[9] M. Seker and E. Zergeroglu, "Nonlinear control of flyback type DC to DC converters: An indirect backstepping approach," *2011 IEEE Inter. Conf. on Control Application*, pp. 65-69, Sep. 2011.

[10] S. C. Tan, Y. M. Lai, and C. K. Tse, "General design issues of sliding-mode controllers in DC-DC converters," *IEEE Trans. Ind. Electron.*, vol. 55, no. 3, pp. 1160-1174, Mar. 2008.

[11] S. C. Tan, Y. M. Lai, and C. K. Tse, "A unified approach to the design of PWM-based sliding-mode voltage controllers for basic DC-DC converters in continuous conduction mode," *IEEE Trans. Circuits Syst. I, Reg. Papers*, vol. 53, no. 8, pp. 1816-1827, Aug. 2006.

[12] S. C. Tan, Y. M. Lai, and C. K. Tse, *Sliding mode control of switching power converters: techniques and implementation*, Boca Raton, FL, USA: CRC Press, 2012.

[13] M. Salimi, J. Soltani, A. Zakipour, and V. Hajbani, "Sliding mode control of the DC-DC flyback converter with zero steady-state error," *4th Power Electron., Drive Systems & Technologies Conf.*, pp. 158-163, Feb. 2013.

[14] M. -T. Lin, "A second order sliding mode controller for the flyback converter," *2014 IEEE Inter. Conf. on Systems, Man and Cybernetics*, pp. 2289-2292, Oct. 2014.

[15] Y. Zhang, M. A. M. Hendrix, and J. L. Duarte, "CCM flyback converter using an observer-based digital controller," *2015 IEEE Inter. Conf. on Industrial Technology*, pp. 2056-2061, Mar. 2015.

[16] S. R. Sanders and G. C. Verghese, "Lyapunov-based control for switched power converters," *IEEE Trans. Power Electron.*, vol. 7, no. 1, pp. 17-24, Jan. 1992.

[17] R. Leyva, A. Cid-Pastor, I. Queinnec, S. Tarbouriech, and L. Martinez-Salamero, "Passivity-based integral control of a boost converter for large-signal stability," *IEE Proc. -Control Theory Appl.*, vol. 153, no. 2, pp. 139-146, Mar. 2006.

[18] H. Komurcugil and O. Kukrer, "A new control strategy for single-phase shunt active power filters using a Lyapunov function," *IEEE Trans. Ind. Electron.*, vol. 53, no. 1, pp. 305-312, Jan. 2006.

[19] S. Rahmani, A. Hamadi, and K. Al-Haddad, "A Lyapunov-function-based control for a three-phase shunt hybrid active filter," *IEEE Trans. Ind. Electron.*, vol. 59, no. 3, pp. 1418-1429, Mar. 2012.

[20] C. Meza, D. Diel, D. Jeltsema, and J. M. A. Scherpen, "Lyapunov-based control scheme for single-phase grid-connected PV central inverters," *IEEE Trans. Control Syst. Technol.*, vol. 20, no. 2, pp. 520-529, Mar. 2012.

[21] H. Komurcugil, N. Altin, S. Ozdemir, and I. Sefa, "An extended Lyapunov-function-based control strategy for single-phase UPS inverters," *IEEE Trans. Power Electron.*, vol. 30, no. 7, pp. 3976-3983, Jul. 2015.

[22] H. Komurcugil, N. Altin, S. Ozdemir, and I. Sefa, "Lyapunov-function and proportional-resonant based control strategy for single-phase grid-connected VSI with LCL filter," *IEEE Trans. Ind. Electron.*, vol. 63, no. 5, pp. 2838-2849, May 2016.

[23] S. K. Sahoo, S. Dasgupta, S. K. Panda, and J. -X. Xu, "A Lyapunov function-based robust direct torque controller for a switched reluctance motor drive system," *IEEE Trans. Power Electron.*, vol. 27, no. 2, pp. 555-564, Feb. 2012.

[24] D. M. van de Sype, K. De Gusseme, A. P. M. Van den Bossche, and J. A. Melkebeek, "Duty-ratio feedforward for digitally controlled boost PFC converters," *IEEE Trans. Ind. Electron.*, vol. 52, no. 1, pp. 108-115, Feb. 2005.

[25] S. -H. Lee, W. -J. Cha, B. -H. Kwon, and M. Kim, "Discrete-

Citation information: DOI 10.1109/TIE.2017.2733459, IEEE

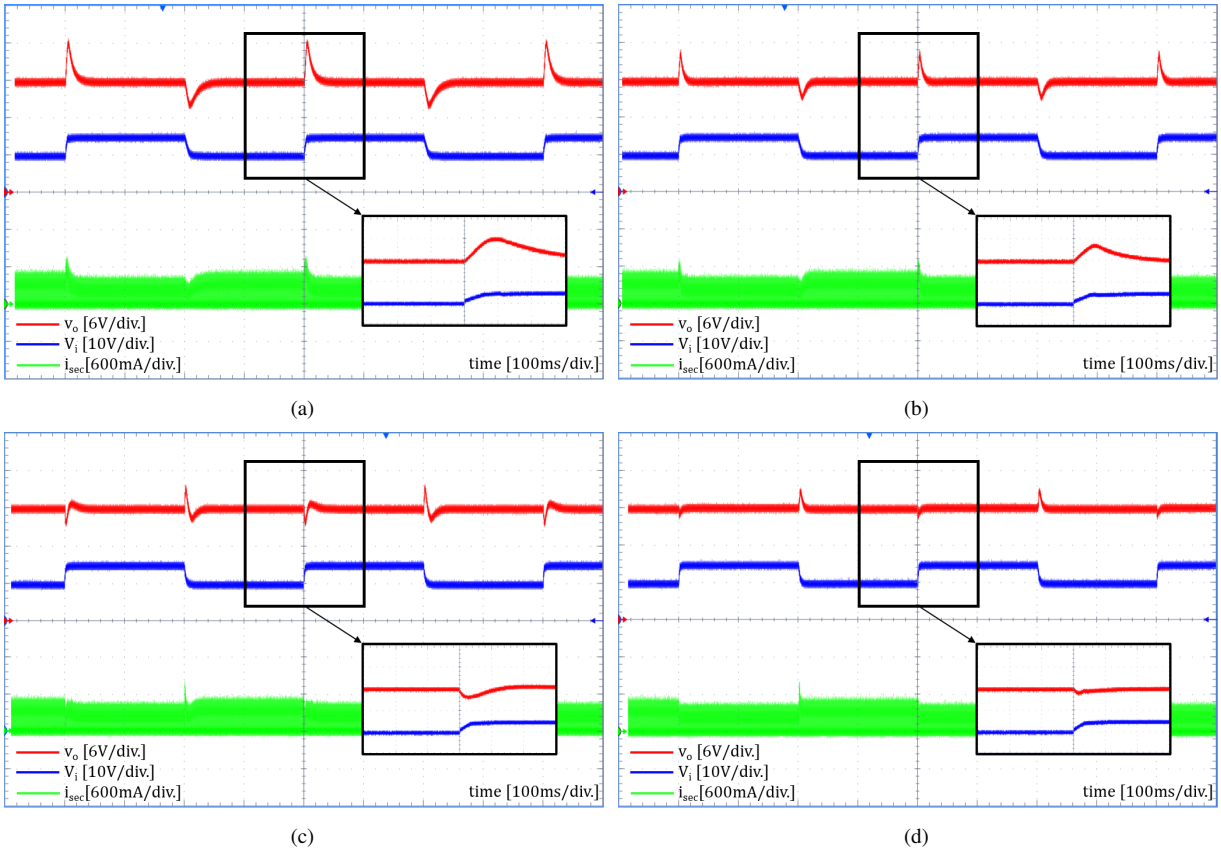

Fig. 10. Experimental waveforms of the flyback CCM converter under input voltage variations. (a) when the voltage-mode controller is used. (b) when the current-mode controller is used. (c) when the sliding mode controller is used. (d) when the proposed controller is used.

time repetitive control of flyback ccm inverter for PV power applications," *IEEE Trans. Ind. Electron.*, vol. 63, no. 2, pp. 976-984, Feb. 2016.

[26] H. Kim, J. S. Lee, J. S. Lai, and M. Kim, "Iterative learning controller with multiple phase-lead compensation for dual-mode flyback inverter," *IEEE Trans. on Power Electron.*, vol. 32, no. 8, pp. 6468-6480, Aug. 2017.

[27] A. Davoudi and J. Jatskevich, "Parasitics realization in state-space average-value modeling of PWM DC-DC converters using an equal area method," *IEEE Trans. Circuits Syst. I, Reg. Papers*, vol. 54, no. 9, , pp. 1960-1967, Sep. 2007.

[28] G. Cimini, G. Ippoliti, G. Orlando, and M. Pirro, "Sensorless power factor control for mixed conduction mode boost converter using passivity-based control," *IET Power Electron.*, vol. 7, no. 12, pp. 2988-2995, Dec. 2014.

[29] H. K. Khalil, *Nonlinear Systems*, Upper Saddle River, NJ, USA: Prentice Hall, 2002.

[30] M. Hallworth and S. A. Shirsavar, "Microcontroller-based peak current mode control using digital slope compensation," *IEEE Trans. on Power Electron.*, vol. 27, no. 7, pp. 3340-3351, Jul. 2012.

[31] S. -C. Tan, Y. M. Lai, C. K. Tse, L. M. Salamero, and C. -K. Wu, "A fast-response sliding-mode controller for boost-type converters with a wide range of operating conditions," *IEEE Trans. Ind. Electron.*, vol. 54, no. 6, pp. 3276-3286, Dec. 2007.

[32] R. -J. Wai and L. -C. Shih, "Design of voltage tracking control for DC-DC boost converter via total sliding-mode technique," *IEEE Trans. Ind. Electron.*, vol. 58, no. 6, pp. 2502-2511, Jun. 2011.

[33] S. H. Chincholkar and C. -Y. Chan, "Design of fixed-frequency pulsewidth-modulation-based sliding-mode controllers for the quadratic boost converter," *IEEE Trans. Circuits Syst. II, Exp. Briefs*, vol. 64, no. 1. pp. 51-55, Jan. 2017.

Seok-Min Wi (S'16) received the B.S degree in electrical engineering from Pohang University of Science and Technology (POSTECH), Pohang, Korea, in 2009, where he is currently pursuing the Ph.D. degree in electrical engineering. His research interests include signal processing of medical device, nonlinear system analysis, and controller design of power system.

Citation information: DOI 10.1109/TIE.2017.2733459, IEEE

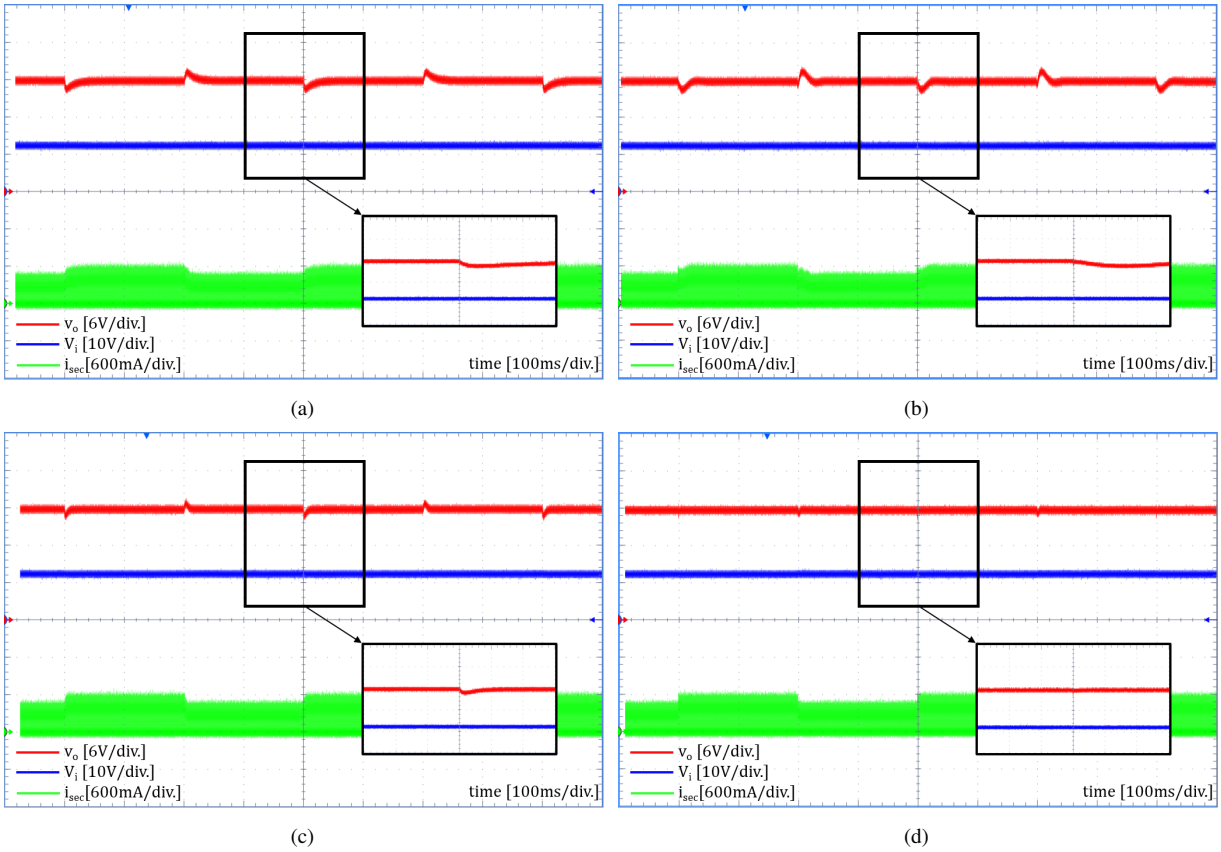

Fig. 11. Experimental waveforms of the flyback CCM converter under output load variations. (a) when the voltage-mode controller is used. (b) when the current-mode controller is used. (c) when the sliding mode controller is used. (d) when the proposed controller is used.

Jin S. Lee (M'85) received the B.S. degree in electronics engineering from Seoul National University, Seoul, Korea, in 1975, the M.S. degree in electrical engineering and computer science from the University of California, Berkeley, in 1980, and the Ph.D. degree in system science from the University of California, Los Angeles, in 1984.

From 1984 to 1985, he worked as a Member of the Technical Staff at AT&T Bell Laboratories, Holmdel, NJ, and, from 1985 to 1989, as a Senior Member of the Engineering Staff at GE Advanced Technology Laboratories, Mt. Laurel, NJ. Since 1989, he has been a Professor at Pohang University of Science and Technology (POSTECH), Pohang, Korea. From 2000 to 2003, he has served as the Dean of Research Affairs at POSTECH. From 2007 to 2012, he also has served as the Dean of Academic Affairs at POSTECH. He is currently the Head of Creative IT Engineering Department and the Director of Future IT Innovation Laboratory at POSTECH. His research interests include nonlinear systems and control, robotics, and intelligent control.

Minsung Kim (M'14) was born in Ulsan, Korea, in 1986. He received the B.S. degree in electrical engineering from Pohang University of Science and Technology (POSTECH), Pohang, Korea, in 2008, and the Ph.D. degree in electrical engineering from POSTECH, Pohang, Korea, in 2013.

Since 2013, he has been with Department of Creative IT Engineering and Future IT Research Laboratory, POSTECH, Pohang, Korea, where he is currently Research Assistant Professor. Since 2016, he has also worked as Research Scholar at Virginia Tech's Future Energy Electronics Center, Blacksburg, VA. His current research interests include renewable energy system, power conversion circuit design, nonlinear system analysis, and controller design for industrial process.

Citation information: DOI 10.1109/TIE.2017.2733459, IEEE

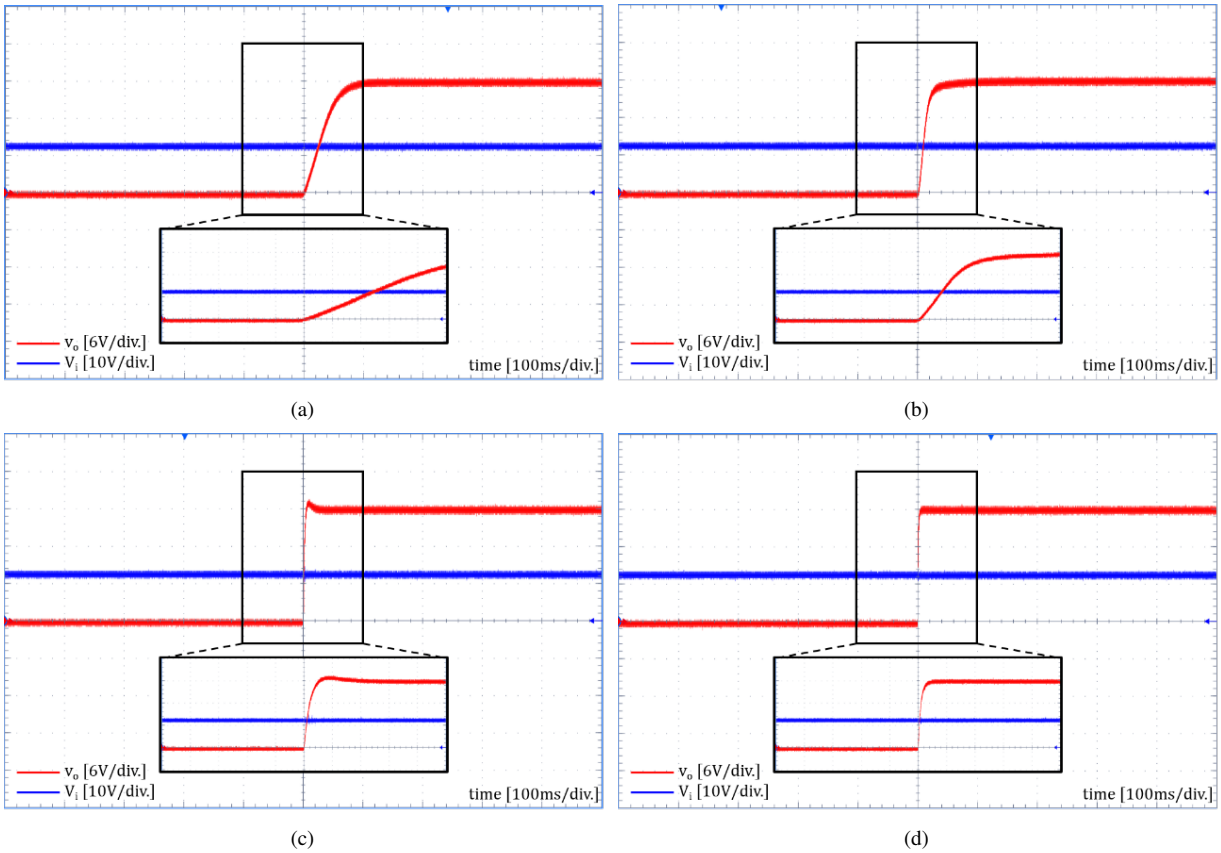

Fig. 12. Experimental waveforms of the flyback CCM converter during system startup. (a) when the voltage-mode controller is used. (b) when the current-mode controller is used. (c) when the sliding mode controller is used. (d) when the proposed controller is used.